A liquid plug moving in an annular pipe—Flow analysis

Yadi Cao, and Ri Li

Citation: Physics of Fluids **30**, 093605 (2018); doi: 10.1063/1.5050258
View online: https://doi.org/10.1063/1.5050258
View Table of Contents: http://aip.scitation.org/toc/phf/30/9
Published by the American Institute of Physics

PHYSICS OF FLUIDS **30**, 093605 (2018)

A liquid plug moving in an annular pipe—Flow analysis

Yadi Cao and Ri Li[a)]
School of Engineering, University of British Columbia, Kelowna, British Columbia V1V 1V7, Canada

(Received 29 July 2018; accepted 3 September 2018; published online 18 September 2018)

The flow in a liquid plug moving in an annular pipe is analytically solved. The interaction with the two concentric walls of the annular pipe results in two toroidal vortexes within the concentric plug. Focus is put on long plugs with aspect ratio $\beta > 2$, which have vortex circulation flow rates and volume ratio independent of the plug length. Based on the analytical results, correlations are derived for the circulation flow rates of the plug and each vortex and for the volume ratio of the two vortexes. Correlations are also developed for evaluating the radial transport of the plug flow. The friction factor for concentric plugs is a function of the aspect ratio and the radius ratio. For very long plugs with $\beta \gg 1$, the friction factor approaches that of the fully developed continuous flow in the annular pipe. *Published by AIP Publishing.* https://doi.org/10.1063/1.5050258

NOMENCLATURE

A_n	coefficient
B_n	coefficient
C_n	coefficient
D_h	hydraulic diameter
D_n	coefficient
f	Darcy friction factor
F	viscous drag force
g	gravitational acceleration rate
g_n	Fourier coefficient
$\mathbf{I}_1$	first order of the first-kind modified Bessel function
$\mathbf{I}_2$	second order of the first-kind modified Bessel function
$\mathbf{K}_1$	first order of the second-kind modified Bessel function
$\mathbf{K}_2$	second order of the second-kind modified Bessel function
l	plug length
p	pressure
Q'	radial flux
$\hat{Q}'_i$	non-dimensional radial flux of inner vortex
$\hat{Q}'_o$	non-dimensional radial flux of outer vortex
r	r-axis in the cylindrical coordinate system
r_i	inner radius of the plug
r_o	outer radius of the plug
$\hat{r}_c$	radial location of the border between the inner and outer vortexes
R	radial location of the pipe wall
u_z	velocity in the z-direction
u_r	velocity in the r-direction
$\hat{\mathbf{u}}$	non-dimensional velocity vector
U	velocity of the plug moving in the pipe
$\hat{V}_i$	non-dimensional volume of the inner vortex
$\hat{V}_o$	non-dimensional volume of the outer vortex
z	z-axis in the cylindrical coordinate system

Symbol

$\hat{}$	non-dimensional

Greek symbols

α_n	eigenvalue
β	aspect ratio
η	radius ratio (or non-dimensional inner radius)
μ	dynamic viscosity
ρ	density
σ	surface tension coefficient
τ	circulation period
ψ	stream function
$\hat{\psi}_o$	maximum of the non-dimensional stream function (outer circulation rate)
$\hat{\psi}_i$	minimum of the non-dimensional stream function
$\lvert\hat{\psi}_i\rvert$	inner circulation rate

Non-dimensional group parameters

Re	Reynolds number based on r_o
Re_{Dh}	Reynolds number based on the hydraulic diameter

I. INTRODUCTION

With the rapid development of microelectronics, microreactors, and micro-electro-mechanical systems (MEMS), the scale of these devices shrinks dramatically, and microfluidics has drawn much attention in recent years.[1] Among all kinds of microfluidics, the hydrodynamics of plug flows is of interest due to their applications in environmental detection,[2] chemical reaction,[3–5] digital flow, and drug delivery.[6] Comparing to continuous flows, the most significant feature of plug flows is the internal circulation,[7,8] which can enhance transport processes such as mass and heat transfers.[9–13]

Generally, there are two categories of plug flows. One category is the liquid-liquid plug flow,[14–17] while the other category is the gas-liquid plug flow.[13,18,19] Most previous studies in the latter category put focus on liquid plugs. Gas-liquid plug flows are common unless more than one liquid flows are required in some specific applications, which then form liquid-liquid plug flows. The present study belongs to the category of gas-liquid plug flows, and the following discussion will be on gas-liquid plug flows only.

a)Author to whom correspondence should be addressed: sunny.li@ubc.ca

Gas-liquid plug flows have been studied experimentally and theoretically. On the experimental side, gas-liquid plug flows have been investigated using non-intrusive methods such as fluorescence and micro PIV (particle imaging velocimetry),[18,19] and most of the experimental work was restricted to straight and slit channels. On the theoretical side, an analytical approach based on the Stokes flow was taken to solve the gas-liquid flow in a 2-D domain.[20] The flow field is constructed by solving a 4th-order PDE (partial differential equation). This method has been proved effective and convenient for plug flows in channels with different shapes, such as 2-D slit channels,[20] curved channels,[21] and circular channels.[22]

Despite varied cross section shapes, channels that have been used for plug flows are single-walled in that the cross section of the channel is one closed curve. However, the annular channel is different as it has two separate walls. Annular channels are commonly seen in many applications, and one major application is the concentric tube (tube-in-tube) heat exchanger.[23–29] There has been much attention to annular flows. Studies have been conducted to investigate one liquid flow[30,31] or two flows[32–36] in annular channels. For plug flows in annular channels, very limited work has been reported. The present work is dedicated to the gas-liquid plug flow in annular pipes. The focus is put on the flow phenomena inside a single liquid plug moving in an annular space confined by two concentric walls. The objective here is not only to analytically solve the flow problem but also to investigate the circulation flow, vortex, pressure drop, and friction.

II. ANALYTICAL SOLUTIONS

Figure 1 schematically shows a liquid plug with a length l moving at a constant velocity U in an annular pipe, which has an inner radius r_i and an outer radius r_o. The fluid properties of the plug that might be relevant to the current study include the density ρ, the dynamic viscosity μ, and the surface tension σ. We drop the surface tension by making the following three assumptions:

(1) The capillary number $\mu U/\sigma \ll 1$;
(2) If the annulus is placed horizontally, the Bond number $\rho g(r_o - r_i)^2/\sigma \ll 1$, where g is the gravitational acceleration rate. If the annulus is placed vertically, $\rho g(r_o - r_i)l/\sigma \ll 1$.

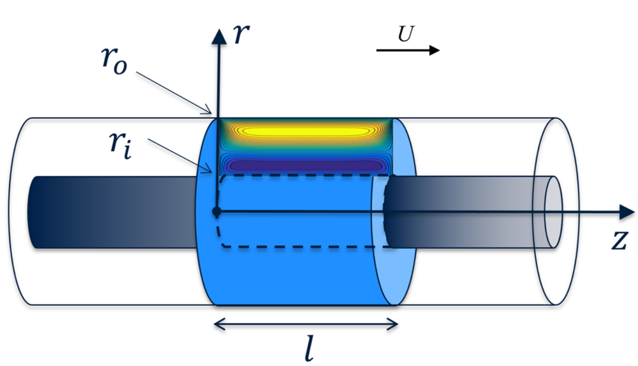

FIG. 1. Schematic of a liquid plug moving in an annular pipe. In the floor-attached frame reference that is not shown, the plug velocity is U.

(3) Both the receding and advancing contact angles are close to 90°.

Due to the above assumptions, the moving plug maintains an axisymmetric shape with the leading and trailing ends being flat. Excluding σ, there remain six parameters, which, according to the Buckingham π theorem, can be represented by three non-dimensional parameters. Here we choose the outer radius r_o as the characteristic length and define three independent non-dimensional parameters, which are

$$\eta = \frac{r_i}{r_o}, \ \hat{l} = \frac{l}{r_o}, \ \mathrm{Re} = \frac{\rho U r_o}{\mu}. \tag{1}$$

Here η is called the radius ratio or the non-dimensional inner radius.

Following the normalization scheme in Eq. (1), we define

$$\hat{z} \equiv \frac{z}{r_o}; \ \hat{r} \equiv \frac{r}{r_o}; \ \hat{u}_z \equiv \frac{u_z}{U}; \ \hat{u}_r \equiv \frac{u_r}{U}. \tag{2}$$

For convenience, the frame of reference is attached to the plug, and the cylindrical coordinate system is chosen, as shown in Fig. 1. The z-axis in the plug-attached frame of reference is set in the direction of the plug moving in the floor-attached frame of reference. The space occupied by the plug is defined by $0 \le \hat{z} \le \hat{l}$ and $\eta \le \hat{r} \le 1$. The remaining spaces, $\hat{z} \le 0$ and $\hat{z} \ge \hat{l}$, are filled with gas.

The general momentum equation for the plug at the steady state is given by

$$\left(\hat{\mathbf{u}} \cdot \hat{\nabla}\right)\hat{\mathbf{u}} = -\hat{\nabla}\hat{p} + \frac{1}{\mathrm{Re}}\hat{\nabla}^2\hat{\mathbf{u}}, \tag{3}$$

where $\hat{\mathbf{u}}$ is in the vectorial form. The non-dimensional pressure is $\hat{p} = p/\rho U^2$. The body force term is not considered due to the assumption that the Froude number $U/\sqrt{g(r_o - r_i)} \gg 1$ for the horizontally placed annular pipe or $U/\sqrt{gl} \gg 1$ for the vertically placed annular pipe.

In the plug-attached frame of reference, non-slip boundary conditions at the plug-wall interfaces appear as a local velocity of $-U$. Hence, the boundary conditions are

$$\hat{u}_z(\hat{z}, 1) = \hat{u}_z(\hat{z}, \eta) = -1. \tag{4}$$

The pipe walls are smooth and impermeable, which requires

$$\hat{u}_r(\hat{z}, 1) = \hat{u}_r(\hat{z}, \eta) = 0. \tag{5}$$

The two ends of the plug are flat and have no mass transfer such as evaporation or condensation. Hence, we can write

$$\hat{u}_z(0, \hat{r}) = \hat{u}_z\left(\hat{l}, \hat{r}\right) = 0. \tag{6}$$

At $\hat{z} = 0$ and $\hat{z} = \hat{l}$, the liquid plug is in contact with the gas fluid. If the gas viscosity is lower than the viscosity of the liquid by orders of magnitude, we may assume the gas flow to be inviscid and write

$$\left.\frac{\partial \hat{u}_r}{\partial \hat{z}}\right|_{\hat{z}=0} = \left.\frac{\partial \hat{u}_r}{\partial \hat{z}}\right|_{\hat{z}=\hat{l}} = 0. \tag{7}$$

The liquid plug is considered incompressible, and the stream function for this axisymmetric flow is

$$\hat{u}_z = \frac{1}{\hat{r}}\frac{\partial \hat{\psi}}{\partial \hat{r}}; \ \hat{u}_r = -\frac{1}{\hat{r}}\frac{\partial \hat{\psi}}{\partial \hat{z}}. \tag{8}$$

The non-dimensional stream function $\hat{\psi}$ and the dimensional stream function ψ are related by

$$\hat{\psi} \equiv \frac{\psi}{r_o^2 U}. \tag{9}$$

Regarding the liquid plug, we further assume that the friction term in Eq. (3) is dominant over the inertia term. To satisfy the assumption, it requires

$$\frac{1^2}{1-\eta} \ll \frac{1}{\mathrm{Re}} \frac{1}{(1-\eta)^2}, \tag{10}$$

which gives

$$\mathrm{Re}(1-\eta) \ll 1. \tag{11}$$

With Eq. (11) being satisfied, Eq. (3) reduces to the Stokes equation given by

$$\hat{\nabla}\hat{p} = \frac{1}{\mathrm{Re}}\hat{\nabla}^2\hat{\mathbf{u}}. \tag{12}$$

By taking curl of Eq. (12) and substituting Eq. (8) into Eq. (12), we have a 4th-order PDE of the stream function, which is

$$\hat{L}_{-1}^4\hat{\psi} = \left(\frac{\partial^2}{\partial\hat{z}^2} + \frac{\partial^2}{\partial\hat{r}^2} - \frac{1}{\hat{r}}\frac{\partial}{\partial\hat{r}}\right)\left(\frac{\partial^2}{\partial\hat{z}^2} + \frac{\partial^2}{\partial\hat{r}^2} - \frac{1}{\hat{r}}\frac{\partial}{\partial\hat{r}}\right)\hat{\psi} = 0. \tag{13}$$

For this 4th-order differential equation, two boundary conditions can be obtained from Eq. (4), which are

$$\frac{1}{\hat{r}}\frac{\partial\hat{\psi}}{\partial\hat{r}}\bigg|_{\hat{r}=\eta} = \frac{1}{\hat{r}}\frac{\partial\hat{\psi}}{\partial\hat{r}}\bigg|_{\hat{r}=1} = -1. \tag{14}$$

Equations (5) and (6) indicate that all the boundary streamlines have a constant stream function value, which, for convenience, is written as

$$\hat{\psi}(\hat{z},\eta) = \hat{\psi}(\hat{z},1) = 0 \tag{15}$$

and

$$\hat{\psi}(0,\hat{r}) = \hat{\psi}\left(\hat{l},\hat{r}\right) = 0. \tag{16}$$

Equation (7) provides another two boundary conditions, which are

$$\frac{\partial^2\hat{\psi}}{\partial\hat{z}^2}\bigg|_{\hat{z}=0} = \frac{\partial^2\hat{\psi}}{\partial\hat{z}^2}\bigg|_{\hat{z}=\hat{l}} = 0. \tag{17}$$

To solve Eq. (13), we consider the Fourier series of the stream function. In view of the boundary conditions at $\hat{z} = 0$ and $\hat{z} = \hat{l}$ defined by Eqs. (16) and (17), the stream function can be written in the Fourier series with only sines involved, which is

$$\hat{\psi} = \sum_{n=1}^{\infty}\hat{\psi}_n = \sum_{n=1}^{\infty} g_n \sin\left(\frac{n\pi}{\hat{l}}\hat{z}\right). \tag{18}$$

The Fourier coefficients g_n are given by

$$g_n = \frac{2}{\hat{l}}\int_0^{\hat{l}}\hat{\psi}\sin\left(\frac{n\pi}{\hat{l}}\hat{z}\right)d\hat{z} = g_n(\hat{r}), \tag{19}$$

which is a function of $\hat{r}$ only.

Substituting Eq. (18) into Eq. (12) gives

$$\left(\frac{d^2}{d\hat{r}^2} - \frac{1}{\hat{r}}\frac{d}{d\hat{r}} - \alpha_n^2\right)\left(\frac{d^2}{d\hat{r}^2} - \frac{1}{\hat{r}}\frac{d}{d\hat{r}} - \alpha_n^2\right)g_n = 0, \tag{20}$$

where $\alpha_n = n\pi/\hat{l}$ is the eigenvalue. Four boundary conditions are needed for solving Eq. (20). Two boundary conditions can be derived from Eq. (14), which are

$$\frac{dg_n}{d\hat{r}}\bigg|_{\hat{r}=\eta} = \frac{dg_n}{d\hat{r}}\bigg|_{\hat{r}=1} = -\frac{2\eta}{\hat{l}\alpha_n}[1-(-1)^n]. \tag{21}$$

Another two boundary conditions are from Eq. (15), which are

$$g_n(\eta) = g_n(1) = 0. \tag{22}$$

The solution of Eq. (20) is

$$g_n = A_n\hat{r}^2\mathbf{I}_2(\alpha_n\hat{r}) + B_n\hat{r}\mathbf{I}_1(\alpha_n\hat{r}) + C_n\hat{r}^2\mathbf{K}_2(\alpha_n\hat{r}) + D_n\hat{r}\mathbf{K}_1(\alpha_n\hat{r}). \tag{23}$$

Here $\mathbf{I}_1$ and $\mathbf{I}_2$ are the first and second order of the first-kind modified Bessel functions, respectively. And $\mathbf{K}_1$ and $\mathbf{K}_2$ are the first and second order of the second-kind modified Bessel functions, respectively. Equation (23) can also be written based on the zeroth and first-order functions.[37] The coefficients, A_n, B_n, C_n, and D_n, should be determined by applying the four boundary conditions given by Eqs. (21) and (22). This can be performed by solving

$$\begin{pmatrix} \eta\mathbf{I}_2(\alpha_n\eta) & \mathbf{I}_1(\alpha_n\eta) & \eta\mathbf{K}_2(\alpha_n\eta) & \mathbf{K}_1(\alpha_n\eta) \\ \mathbf{I}_2(\alpha_n) & \mathbf{I}_1(\alpha_n) & \mathbf{K}_2(\alpha_n) & \mathbf{K}_1(\alpha_n) \\ \eta\mathbf{I}_1(\alpha_n\eta) & \mathbf{I}_0(\alpha_n\eta) & -\eta\mathbf{K}_1(\alpha_n\eta) & -\mathbf{K}_0(\alpha_n\eta) \\ \mathbf{I}_1(\alpha_n) & \mathbf{I}_0(\alpha_n) & -\mathbf{K}_1(\alpha_n) & -\mathbf{K}_0(\alpha_n) \end{pmatrix}\begin{pmatrix} A_n \\ B_n \\ C_n \\ D_n \end{pmatrix} = \begin{pmatrix} 0 \\ 0 \\ -\frac{2\eta}{\hat{l}\alpha_n}[1-(-1)^n] \\ -\frac{2\eta}{\hat{l}\alpha_n}[1-(-1)^n] \end{pmatrix}, \tag{24}$$

where Cramer's rule has been used. Clearly, A_n, B_n, C_n, and D_n are zero if n is even.

Finally, the analytical solution of the stream function is

$$\hat{\psi}(\hat{z},\hat{r}) = \sum_{n=1,3,5\ldots}^{\infty}[A_n\hat{r}^2\mathbf{I}_2(\alpha_n\hat{r}) + B_n\hat{r}\mathbf{I}_1(\alpha_n\hat{r}) + C_n\hat{r}^2\mathbf{K}_2(\alpha_n\hat{r}) + D_n\hat{r}\mathbf{K}_1(\alpha_n\hat{r})]\sin(\alpha_n\hat{z}). \tag{25}$$

Substituting Eq. (25) into Eq. (8) gives the velocity solutions, which are

$$\hat{u}_z(\hat{z},\hat{r}) = \sum_{n=1,3,5\ldots}^{\infty}\alpha_n[A_n\hat{r}\mathbf{I}_1(\alpha_n\hat{r}) + B_n\mathbf{I}_0(\alpha_n\hat{r}) - C_n\hat{r}\mathbf{K}_1(\alpha_n\hat{r}) - D_n\mathbf{K}_0(\alpha_n\hat{r})]\sin(\alpha_n\hat{z}), \tag{26}$$

$$\hat{u}_r(\hat{z},\hat{r}) = \sum_{n=1,3,5\ldots}^{\infty}-\alpha_n[A_n\hat{r}\mathbf{I}_2(\alpha_n\hat{r}) + B_n\mathbf{I}_1(\alpha_n\hat{r}) + C_n\hat{r}\mathbf{K}_2(\alpha_n\hat{r}) + D_n\mathbf{K}_1(\alpha_n\hat{r})]\cos(\alpha_n\hat{z}). \tag{27}$$

The pressure solution can be obtained by applying Eqs. (26) and (27) to Eq. (12) with the given pressure boundary conditions and the Reynolds number Re. The pressure drop and friction factor will be discussed in Sec. V.

III. CIRCULATION AND VORTEXES

The stream function given by Eq. (25) is plotted in Fig. 2 for three plugs, which have varied values of η and $\hat{l}$. Two toroidal vortexes are formed inside the plug: the one close to the outer wall is called the *outer vortex*, and the one close to the inner wall is called the *inner vortex*. The inner vortex is smaller than the outer vortex. As η increases, the difference diminishes. The two vortexes are in contact at $\hat{r} = \hat{r}_c$, where the streamline $\hat{\psi} = 0$. The outer vortex is located at $\hat{r} > \hat{r}_c$, where $\hat{\psi} > 0$. The maximum of $\hat{\psi}$ is denoted by $\hat{\psi}_o$, which is the non-dimensional circulation flow rate of the outer vortex, in short called the *outer circulation rate*. It should be noted that the dimensional outer circulation rate $\psi_o = \hat{\psi}_o r_o^2 U_0^2$ is the volume flow rate per unit radian of the polar angle. The inner vortex is located at $\hat{r} < \hat{r}_c$, where $\hat{\psi} < 0$. The minimum of $\hat{\psi}$ is denoted by $\hat{\psi}_i$, and the circulation flow rate of the inner vortex is $\left|\hat{\psi}_i\right|$, in short called the *inner circulation rate*.

The range of the stream function, $\hat{\psi}_o - \hat{\psi}_i$, is the circulation flow rate of the entire plug, in short called the *plug circulation rate*. Figure 3(a) shows that the plug circulation rate increases with the length $\hat{l}$ when $\hat{l}$ is small and eventually becomes independent of $\hat{l}$. The inner radius η shows more effect on the circulation flow rate. As η increases from 0 to 1, the flow rate reduces toward zero. The two vortexes are compared using $\left|\hat{\psi}_i/\hat{\psi}_o\right|$, which is plotted in Fig. 3(b). The ratio decreases with increasing $\hat{l}$ for short plugs, and it becomes independent of $\hat{l}$ for long plugs. When η is small, the plug circulation is dominated by the outer vortex. As η increases, the difference of the circulation rate between the two vortexes decreases.

The two vortexes border at $\hat{r} = \hat{r}_c$, which can be determined from the volume ratio of the two vortexes using

$$\frac{\hat{V}_i}{\hat{V}_o} = \frac{\hat{r}_c^2 - \eta^2}{1 - \hat{r}_c^2}, \tag{28}$$

where $\hat{V}_i$ and $\hat{V}_o$ are the non-dimensional volumes of the inner vortex and outer vortex, respectively, which have been normalized by the volume of the plug. The volume ratio is plotted in Fig. 4, which shows that the inner vortex is always smaller than the outer vortex. For short plugs, the volume ratio decreases with increasing $\hat{l}$, while for long plugs, the volume ratio is independent of $\hat{l}$.

Figures 3 and 4 show that the circulation rates and the volume ratios are dependent on $\hat{l}$ for short plugs but independent of $\hat{l}$ for long plugs. However, the ranges of $\hat{l}$ for the short and long plugs vary with η. To determine the short and long plugs, we introduce

$$\beta = \frac{l}{r_o - r_i} = \frac{\hat{l}}{1 - \eta}, \tag{29}$$

which is called the *aspect ratio*. In Fig. 5, the plug circulation rate is plotted versus the aspect ratio. As shown by the inset in Fig. 5, $\left(\hat{\psi}_o - \hat{\psi}_i\right)_{max}$ is the circulation rate of long plugs, which is independent of $\hat{l}$. Figure 5 shows that, regardless of

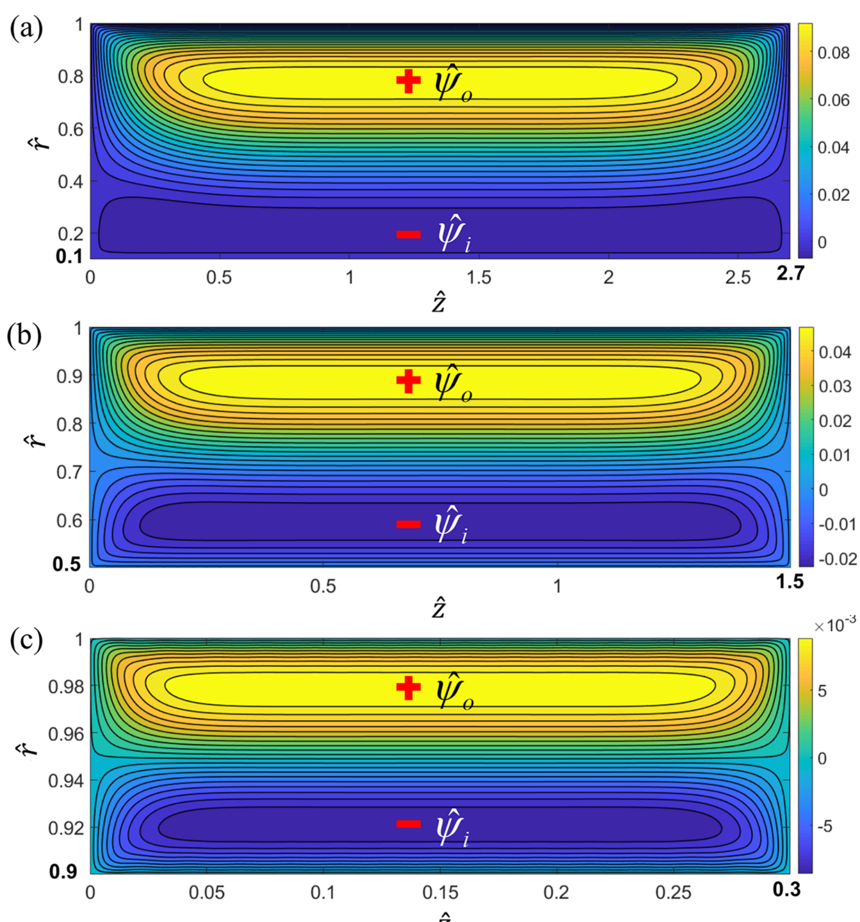

FIG. 2. Streamlines of three plugs: (a) $\eta = 0.1$, $\hat{l} = 2.7$; (b) $\eta = 0.5$, $\hat{l} = 1.5$; and (c) $\eta = 0.9$, $\hat{l} = 0.3$. In the floor-attached frame of reference, the plugs are moving from left to right.

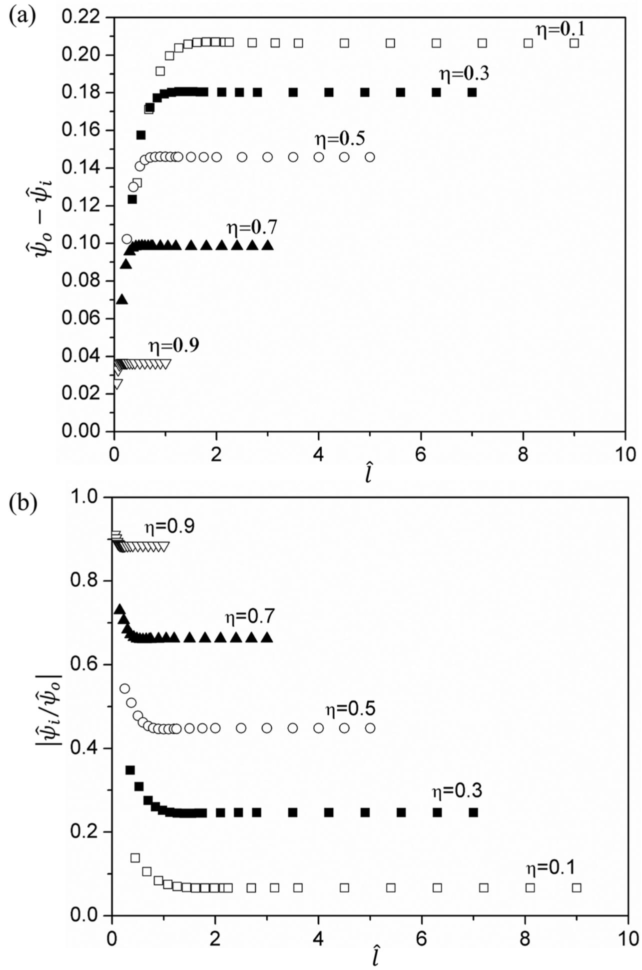

FIG. 3. (a) Plug circulation rate and (b) circulation rate ratio of the inner vortex to the outer vortex.

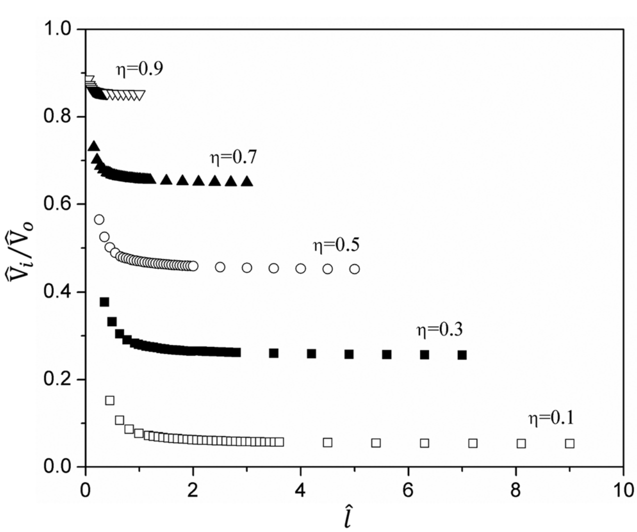

FIG. 4. Volume ratio of the inner vortex to the outer vortex.

η, $\hat{\psi}_o - \hat{\psi}_i$ is within less than 1% difference from $\left(\hat{\psi}_o - \hat{\psi}_i\right)_{max}$ for $\beta > 2$. Similar trends can be observed if the data of the circulation rate ratio in Fig. 3(b) and the data of volume ratio in Fig. 4 are plotted against β. Hence, plugs with aspect ratio $\beta > 2$ are considered as long plugs.

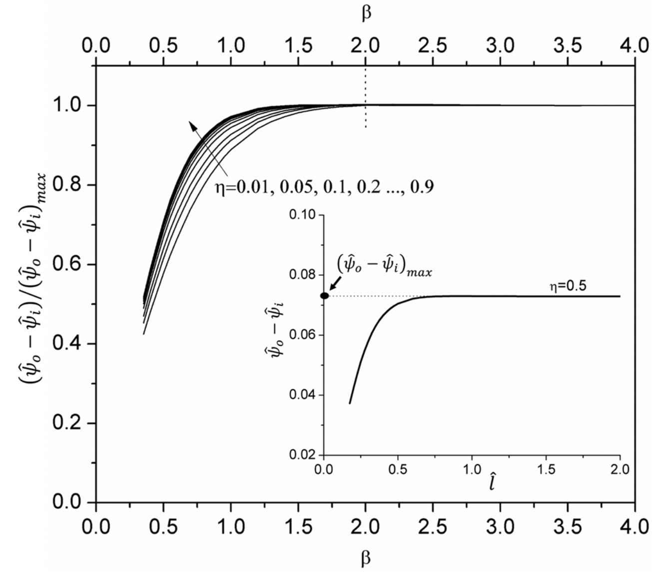

FIG. 5. Plug circulation rate is independent of $\hat{l}$ for $\beta > 2$. Here data points are plotted as lines instead of scattered symbols. The data presented in Fig. 3 are included.

IV. CIRCULATION IN LONG PLUGS ($\beta > 2$)

The analysis in this section will focus on long plugs, which have relatively large aspect ratios, i.e., $\beta > 2$. To focus on long plugs is mainly because the assumption of flat-ended plugs is reasonable only for long plugs. As shown above, the circulation flow rates and the volume ratio of the two vortexes are dependent on η only. Correlations will be derived in this section.

Equation (25) is applied to long plugs with varied inner radii η and lengths $\hat{l}$. The inner radius η is varied between 0 and 1, while $\hat{l}$ is changed accordingly to ensure $\beta > 2$. The maxima and minima of the stream function $\hat{\psi}$ are determined to obtain the circulation flow rates of the outer vortex, the inner vortex, and the plug, which are $\hat{\psi}_o$, $\left|\hat{\psi}_i\right|$, and $\hat{\psi}_o - \hat{\psi}_i$, respectively. The three circulation rates are plotted in Fig. 6. The plug circulation

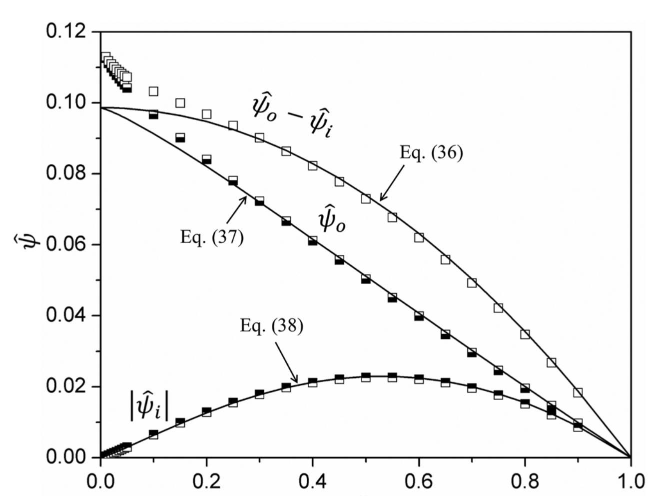

FIG. 6. Plug circulation rate, inner circulation rate, and outer circulation rate of long plugs ($\beta > 2$). Scattered symbols are the data from Eq. (25). Solid lines are plotted using derived correlation equations as indicated.

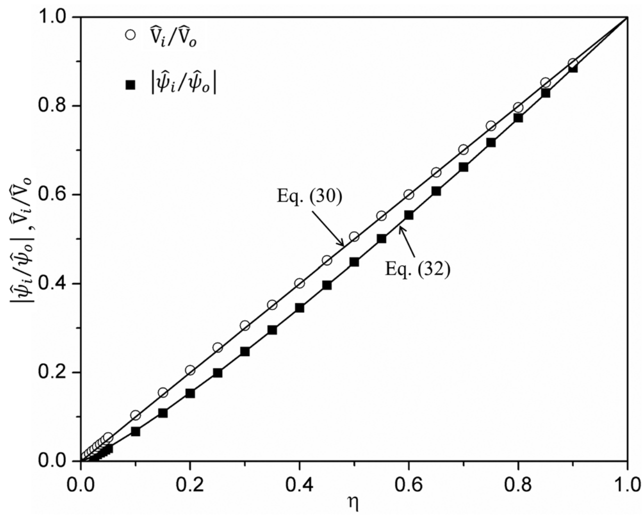

FIG. 7. Circulation rate ratio and volume ratio of long plugs ($\beta > 2$). Scattered symbols are data obtained from Eq. (25). Solid lines are curve-fitting lines corresponding to the equations as indicated.

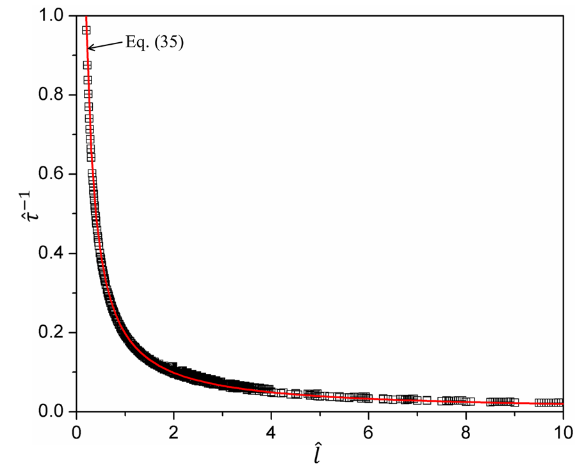

FIG. 8. Circulation frequency of long plugs ($\beta > 2$). Scattered data points with varied η and $\hat{l}$ are obtained from Eqs. (25) and (34). Curve fitting results in Eq. (35).

decreases as η increases. If $\eta = 1$ (i.e., $r_i = r_o$), the flow rate is zero as there is no flow area. The inner circulation is zero if $\eta = 0$. The relationship of the three circulation rates with η will be derived later.

The two vortexes in long plugs are compared in Fig. 7, where the circulation flow rate ratio $\left|\hat{\psi}_i/\hat{\psi}_o\right|$ and the volume ratio $\hat{V}_i/\hat{V}_o$ are plotted against η. The volume ratio of the two vortexes shows a linear relationship with the radius ratio of the plug, which is

$$\frac{V_i}{V_o} = \eta. \tag{30}$$

Combining Eqs. (28) and (30) gives the border location of the two vortexes, which is

$$\hat{r}_c = \eta^{0.5}. \tag{31}$$

Similarly, Fig. 7 shows that the circulation rate ratio of the two vortexes changes with η following

$$\left|\frac{\hat{\psi}_i}{\hat{\psi}_o}\right| = \eta^{1.16}. \tag{32}$$

To further analyze the plug circulation, we introduce the *circulation period*, denoted by τ, during which the circulated volume of fluid is equal to the plug volume. For convenience, we use τ^{-1}, called the *circulation frequency*. The definition of the circulation frequency is

$$\tau^{-1} = \frac{2\pi\left(\hat{\psi}_o - \hat{\psi}_i\right)r_o^2 U}{\pi\left(r_o^2 - r_i^2\right)l}. \tag{33}$$

Applying rearrangement gives the circulation frequency in its non-dimensional form, which is

$$\hat{\tau}^{-1} = \left(\frac{\tau U}{r_o}\right)^{-1} = \frac{2\left(\hat{\psi}_o - \hat{\psi}_i\right)}{(1-\eta^2)\hat{l}}. \tag{34}$$

The non-dimensional circulation frequency is plotted against the length $\hat{l}$ in Fig. 8. Applying curve fitting gives

$$\hat{\tau}^{-1} = 0.1973\hat{l}^{-1}. \tag{35}$$

Equation (35) shows that the frequency is inversely proportional to the plug length and that the frequency is independent of the inner radius η.

Combining Eqs. (34) and (35) gives the correlation for the plug circulation rate of long plugs, which is

$$\hat{\psi}_o - \hat{\psi}_i = 0.0986\left(1 - \eta^2\right). \tag{36}$$

Combining Eq. (36) and Eq. (32), we obtain the correlation for the outer circulation rate of long plugs, which is

$$\hat{\psi}_o = \frac{0.0986\left(1-\eta^2\right)}{1+\eta^{1.16}}. \tag{37}$$

And the correlation for the inner circulation rate of long plugs is

$$\left|\hat{\psi}_i\right| = \frac{0.0986\left(1-\eta^2\right)\eta^{1.16}}{1+\eta^{1.16}}. \tag{38}$$

Equations (36)–(38) are plotted in Fig. 6. For the inner vortex, Eq. (38) shows good agreement with the data points. For the outer vortex, Eq. (37) agrees well with the data points except for plugs with small inner radius, $\eta <\sim 0.2$. As a result, Eq. (36) predicts the plug circulation rate with good accuracy except for small inner radii.

The major difference between the plug flow and the continuous flow in an annular pipe is the circulation flow inside the plug. The circulation results in transport in the radial direction, which does not exist in the fully developed continuous flow. The radial transport can be characterized by

$$Q' = \frac{\left(\hat{\psi}_o - \hat{\psi}_i\right)r_o^2 U}{l/2}, \tag{39}$$

which is the plug circulation rate divided by half plug length. Here Q' is a volumetric flow rate per unit radian of the polar angle and per unit length and is called the *radial flux*. We further non-dimensionalize Eq. (39) and substitute Eq. (36) into Eq. (39) and get

$$\hat{Q}' = \frac{Q'}{r_o U} = \frac{2\left(\hat{\psi}_o - \hat{\psi}_i\right)}{\hat{l}} = 0.1973\hat{l}^{-1}\left(1-\eta^2\right). \tag{40}$$

Equation (40) shows that the radial flux decreases with increasing the plug length and/or increasing the inner radius.

Similar to Eq. (40), the radial flux of the inner vortex can be evaluated using

$$\hat{Q}_i' = \frac{2\left|\hat{\psi}_i\right|}{\hat{l}} = \frac{0.1973\left(1-\eta^2\right)\eta^{1.16}}{\left(1+\eta^{1.16}\right)\hat{l}}. \tag{41}$$

The radial flux of the outer vortex can be evaluated using

$$\hat{Q}_o' = \frac{2\hat{\psi}_o}{\hat{l}} = \frac{0.1973\left(1-\eta^2\right)}{\left(1+\eta^{1.16}\right)\hat{l}}. \tag{42}$$

Equations (40)–(42) are useful for studying transport processes such as heat transfer of the plug flow.

V. FRICTION FACTOR

Here we will focus on the viscous friction of the liquid plug and derive the friction factor for concentric plugs. The viscous drag force on a plug moving in an annular pipe is

$$F = -2\pi\mu\left[R\int_0^l\left(\frac{\partial u_z}{\partial r}\right)_{r=R}dz\right]\Bigg|_{R=r_i}^{R=r_o}. \tag{43}$$

Here R is the radial location of the pipe wall. The minus sign on the left indicates that the force is opposite to the plug motion and in the negative z direction (see Fig. 1). Applying force balance to the plug, the pressure drop in the z direction across the plug is

$$\begin{aligned}\Delta\hat{p} &= \frac{\Delta p}{\rho U^2} = \frac{F}{\pi\left(r_o^2-r_i^2\right)\rho U^2}\\ &= -\frac{2}{\mathrm{Re}(1-\eta^2)}\left[\hat{R}\int_0^{\hat{l}}\left(\frac{\partial\hat{u}_z}{\partial\hat{r}}\right)_{\hat{r}=\hat{R}}d\hat{z}\right]\Bigg|_{\hat{R}=\eta}^{\hat{R}=1}.\end{aligned} \tag{44}$$

The hydraulic diameter of the plug is $D_h = 2(r_o - r_i)$, and the Reynolds number based on the hydraulic diameter is

$$\mathrm{Re}_{D_h} = \frac{\rho U D_h}{\mu} = 2(1-\eta)\,\mathrm{Re}, \tag{45}$$

where the other Reynolds number defined in Eq. (1) has been used. The Darcy friction factor is defined as

$$f = \frac{-(\Delta p/l)D_h}{\rho U^2/2} = -4\frac{\Delta\hat{p}}{\beta}, \tag{46}$$

where the definition of the aspect ratio, Eq. (29), has been used. Substituting Eq. (44) into Eq. (46) gives

$$\begin{aligned} f\mathrm{Re}_{D_h} = \frac{32}{\beta(1+\eta)}\sum_{n=1,3,5\ldots}^{\infty}&\alpha_n\left[A_n\hat{R}^2\mathbf{I}_0\left(\alpha_n\hat{R}\right)+B_n\hat{R}\mathbf{I}_1\left(\alpha_n\hat{R}\right)\right.\\ &\left.+C_n\hat{R}^2\mathbf{K}_0\left(\alpha_n\hat{R}\right)+D_n\hat{R}\mathbf{K}_1\left(\alpha_n\hat{R}\right)\right]\Big|_{\hat{R}=\eta}^{\hat{R}=1}.\end{aligned} \tag{47}$$

Equation (47) is applied to plugs with varied values of aspect ratio β and radius ratio η, and the results are plotted in Fig. 9. Generally, $f\mathrm{Re}_{D_h}$ decreases with increasing β and increases with increasing η. As β becomes big, $f\mathrm{Re}_{D_h}$ approaches a steady value specific for a given η.

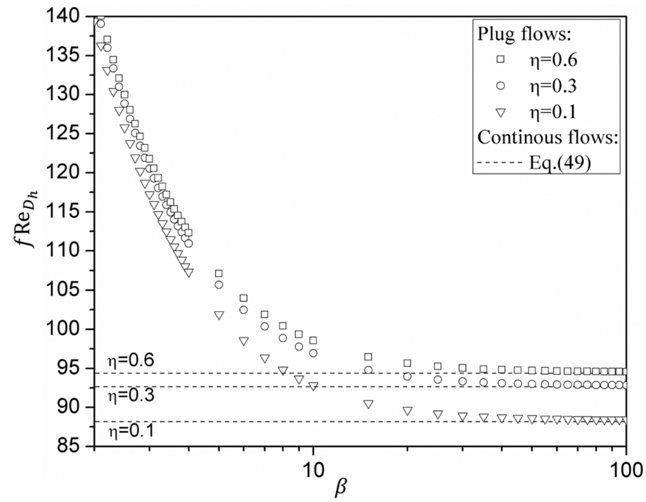

FIG. 9. Friction factor of plugs with varied aspect ratios and radius ratios.

If a plug is very long, i.e., $\beta \to \infty$, the flow approaches a continuous annulus flow. The solution for a fully developed continuous flow in an annular pipe[38] is

$$\hat{u}_z = \frac{2\left(1-\hat{r}^2\right)\ln\eta - 2\left(1-\eta^2\right)\ln\hat{r}}{(1-\eta^2)+(1+\eta^2)\ln\eta} - 1. \tag{48}$$

In a similar fashion to Eqs. (43)–(47), the friction factor for the continuous annulus flow is

$$f\mathrm{Re}_{D_h} = \frac{64(1-\eta)^2\ln\eta}{(1-\eta^2)+(1+\eta^2)\ln\eta}. \tag{49}$$

As shown in Fig. 9, Eq. (49) agrees with the steady values of $f\mathrm{Re}_{D_h}$ for long plugs.

To further compare the friction factor of plug flows with continuous flows, Eq. (47) is plotted versus the radius ratio for long plugs ($\beta = 10$ and 100) in comparison with Eq. (49), as shown in Fig. 10. Plugs with $\beta = 100$ behave like continuous flows as their friction factor values match well with those of the continuous flows. Both Eq. (47) and Eq. (49) also match with other laminar flows in tubes with different cross sections.[39]

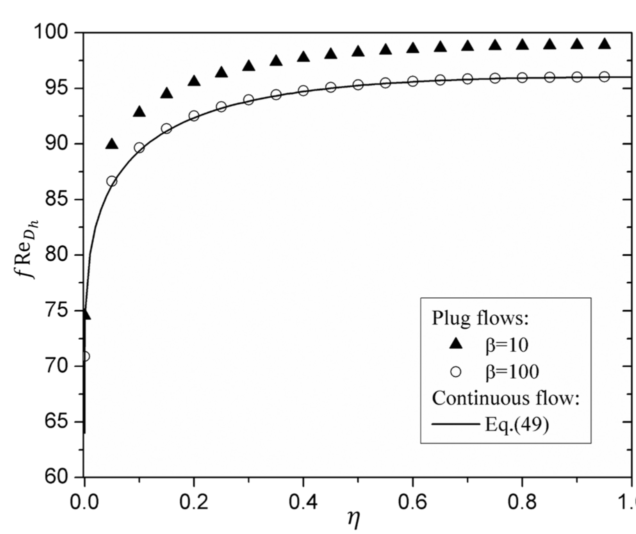

FIG. 10. Friction factors of long plugs in comparison with those of continuous annulus flows with varied radius ratios.

Figure 10 shows that as $\eta \to 0, f\mathrm{Re}_{D_h}$ approaches 64, which is for the circular pipe flow. As $\eta \to 1, f\mathrm{Re}_{D_h}$ approaches 96, which is for the flow between two parallel plates.

From the results shown in Figs. 9 and 10, it can be concluded that the flow in a very long plug is the same as the continuous flow. In a continuous annulus flow, if we move in the flow direction at a speed equal to the mean flow velocity, we should be able to observe streamlines similar to those shown in Fig. 2, but the observed streamlines are all horizontal and parallel and are infinite in the z direction.

VI. SUMMARY

The Stokes equation is solved for a liquid plug moving in an annular pipe. By plotting the stream function solution, we observe two toroidal vortexes due to the friction on the two concentric walls. It is found that the circulation flow rates and the volume ratio of the two vortexes change with the plug length for short plugs and become independent of the plug length for long plugs. It is found that plugs can be considered long if its aspect ratio is larger than 2.

Focus is put on long plugs. The circulation rate ratio and the volume ratio of the two vortexes show simple relationships with respect to the inner radius. The circulation frequency is found to be independent of the inner radius. Based on the curve fitting equations, correlations for plug, inner, and outer circulation rates are derived. Furthermore, the radial flux is introduced and its correlations are developed for evaluating the radial transport of the plug flow. The correlations are useful for applications based on plug flows. For example, they can be used for designing plug-flow concentric tube (tube-in-tube) heat exchangers.

The friction factor of the concentric plug is a function of the aspect ratio and radius ratio. When the plug is very long, i.e., $\beta \gg 1$, the plug flow behaves like the continuous flow. When the radius ratio approaches zero or unity, the derived friction factors match with those of the circular pipe flow and the flow between parallel plates.

ACKNOWLEDGMENTS

The authors thank the Natural Sciences and Engineering Research Council of Canada (NSERC) for support. The first author would like to thank Dr. Xuan Gao for his suggestions at the beginning of this work.

[1] H. A. Stone, A. D. Stroock, and A. Ajdari, "Engineering flows in small devices: Microfluidics toward a lab-on-a-chip," Annu. Rev. Fluid Mech. **36**(1), 381–411 (2004).
[2] S. Lansing, J. Viquez, H. Martinez, R. Botero, and J. Martin, "Quantifying electricity generation and waste transformations in a low-cost, plug-flow anaerobic digestion system," Ecol. Eng. **34**(4), 332–348 (2008).
[3] M. T. Kreutzer, F. Kapteijn, J. A. Moulijn, and J. J. Heiszwolf, "Multiphase monolith reactors: Chemical reaction engineering of segmented flow in microchannels," Chem. Eng. Sci. **60**(22), 5895–5916 (2005).
[4] S. Lansing, J. F. Martin, R. B. Botero, T. N. da Silva, and E. D. da Silva, "Methane production in low-cost, unheated, plug-flow digesters treating swine manure and used cooking grease," Bioresour. Technol. **101**(12), 4362–4370 (2010).
[5] B. K. Yen, A. Gunther, M. A. Schmidt, K. F. Jensen, and M. G. Bawendi, "A microfabricated gas-liquid segmented flow reactor for high-temperature synthesis: The case of CdSe quantum dots," Angew. Chem., Int. Ed. **44**(34), 5447–5451 (2005).
[6] R. Sista, Z. Hua, P. Thwar, A. Sudarsan, V. Srinivasan, A. Eckhardt, M. Pollack, and V. Pamula, "Development of a digital microfluidic platform for point of care testing," Lab Chip **8**(12), 2091–2104 (2008).
[7] P. Angeli and A. Gavriilidis, "Hydrodynamics of Taylor flow in small channels: A review," Proc. Inst. Mech. Eng., Part C **222**(5), 737–751 (2008).
[8] W. B. Kolb and R. L. Cerro, "The motion of long bubbles in tubes of square cross-section," Phys. Fluids A **5**(7), 1549–1557 (1993).
[9] Z. Che, N. T. Nguyen, and T. N. Wong, "Analysis of chaotic mixing in plugs moving in meandering microchannels," Phys. Rev. E **84**(6), 066309 (2011).
[10] A. Asthana, I. Zinovik, C. Weinmueller, and D. Poulikakos, "Significant Nusselt number increase in microchannels with a segmented flow of two immiscible liquids: An experimental study," Int. J. Heat Mass Transfer **54**, 1456–1464 (2011).
[11] Z. Che, T. N. Wong, and N.-T. Nguyen, "Heat transfer enhancement by recirculating flow within liquid plugs in microchannels," Int. J. Heat Mass Transfer **55**, 1947–1956 (2012).
[12] Z. Che, T. N. Wong, and N.-T. Nguyen, "Heat transfer in plug flow in cylindrical microcapillaries with constant surface heat flux," Int. J. Therm. Sci. **64**, 204–212 (2013).
[13] J. Zhang, D. F. Fletcher, and W. Li, "Heat transfer and pressure drop characteristics of gas–liquid Taylor flow in mini ducts of square and rectangular cross-sections," Int. J. Heat Mass Transfer **103**, 45–56 (2016).
[14] A. Ghaini, A. Mescher, and D. W. Agar, "Hydrodynamic studies of liquid–liquid slug flows in circular microchannels," Chem. Eng. Sci. **66**(6), 1168–1178 (2011).
[15] M. N. Kashid, I. Gerlach, S. Goetz, J. Franzke, J. F. Acker, F. Platte, D. W. Agar, and S. Turek, "Internal circulation within the liquid slugs of a liquid–liquid slug-flow capillary microreactor," Ind. Eng. Chem. Res. **44**(14), 5003–5010 (2005).
[16] R. Gupta, S. S. Y. Leung, R. Manica, D. F. Fletcher, and B. S. Haynes, "Hydrodynamics of liquid–liquid Taylor flow in microchannels," Chem. Eng. Sci. **92**, 180–189 (2013).
[17] S. K. R. Cherlo, S. Kariveti, and S. Pushpavanam, "Experimental and numerical investigations of two-phase (liquid–liquid) flow behavior in rectangular microchannels," Ind. Eng. Chem. Res. **49**(2), 893–899 (2010).
[18] A. Gunther, S. A. Khan, M. Thalmann, F. Trachsel, and K. F. Jensen, "Transport and reaction in microscale segmented gas-liquid flow," Lab Chip **4**(4), 278–286 (2004).
[19] C. Meyer, M. Hoffmann, and M. Schlüter, "Micro-PIV analysis of gas–liquid Taylor flow in a vertical oriented square shaped fluidic channel," Int. J. Multiphase Flow **67**, 140–148 (2014).
[20] J. Sivasamy, Z. Che, T. Neng Wong, N.-T. Nguyen, and L. Yobas, "A simple method for evaluating and predicting chaotic advection in microfluidic slugs," Chem. Eng. Sci. **65**(19), 5382–5391 (2010).
[21] Z. Che, T. N. Wong, and N.-T. Nguyen, "An analytical model for a liquid plug moving in curved microchannels," Int. J. Heat Mass Transfer **53**, 1977–1985 (2010).
[22] Z. Che, T. N. Wong, and N.-T. Nguyen, "An analytical model for plug flow in microcapillaries with circular cross section," Int. J. Heat Fluid Flow **32**(5), 1005–1013 (2011).
[23] C. Hong, Y. Asako, and K. Suzuki, "Convection heat transfer in concentric micro annular tubes with constant wall temperature," Int. J. Heat Mass Transfer **54**, 5242–5252 (2011).
[24] A. F. Khadrawi and A. Al-Shyyab, "Slip flow and heat transfer in axially moving micro-concentric cylinders," Int. Commun. Heat Mass Transfer **37**(8), 1149–1152 (2010).
[25] P. Naphon, "Study on the exergy loss of the horizontal concentric micro-fin tube heat exchanger," Int. Commun. Heat Mass Transfer **38**(2), 229–235 (2011).
[26] P. Naphon and T. Suchana, "Heat transfer enhancement and pressure drop of the horizontal concentric tube with twisted wires brush inserts," Int. Commun. Heat Mass Transfer **38**(2), 236–241 (2011).
[27] M. Shojaeian, M. Yildiz, and A. Koşar, "Heat transfer characteristics of plug flows with temperature-jump boundary conditions in parallel-plate channels and concentric annuli," Int. J. Therm. Sci. **84**, 252–259 (2014).
[28] B.-X. Wang and X.-Z. Du, "Condensation on the outside surface of a small/mini diameter tube for vapor flowing through a horizontal annulus surround by an adiabatic concentric tube," Int. J. Heat Mass Transfer **43**(8), 1391–1398 (2000).
[29] M. Turkyilmazoglu, "Anomalous heat transfer enhancement by slip due to nanofluids in circular concentric pipes," Int. J. Heat Mass Transfer **85**, 609–614 (2015).
[30] H. V. Moradi and J. M. Floryan, "On the mixing enhancement in annular flows," Phys. Fluids **29**(2), 024106 (2017).

[31] G. A. Messaris and G. T. Karahalios, "Unsteady fluid flow in a slightly curved annular pipe: The impact of the annulus on the flow physics," Phys. Fluids **29**(2), 021903 (2017).
[32] Z. Ding, R. Liu, and Z. Liu, "Interfacial instabilities in two immiscible flows in an annular duct: Shear-thinning fluids surrounded with Newtonian fluids," Phys. Fluids **29**(5), 053101 (2017).
[33] S. Tripathi, R. F. Tabor, R. Singh, and A. Bhattacharya, "Characterization of interfacial waves and pressure drop in horizontal oil-water core-annular flows," Phys. Fluids **29**(8), 082109 (2017).
[34] G. Chattopadhyay, R. Usha, and K. C. Sahu, "Core-annular miscible two-fluid flow in a slippery pipe: A stability analysis," Phys. Fluids **29**(9), 097106 (2017).
[35] P. Kumar, A. K. Das, and S. K. Mitra, "Physical understanding of gas-liquid annular flow and its transition to dispersed droplets," Phys. Fluids **28**(7), 072101 (2016).
[36] H. Zhang, A. Nikolov, J. Feng, and D. Wasan, "The dynamics of the annular liquid layer inside a cylindrical capillary," Phys. Fluids **28**(2), 024107 (2016).
[37] G. Brenn, *Analytical Solutions for Transport Processes* (Springer, New York, 2016).
[38] W. E. Langlois and M. O. Deville, *Slow Viscous Flow* (Springer, 1964).
[39] R. K. Shah and A. L. London, *Laminar Flow Forced Convection in Ducts: A Source Book for Compact Heat Exchanger Analytical Data* (Academic Press, 2014).